Numerical study of the quantum valley Hall effect

S. K. Wang, Jun Wang,* and Jun-Feng Liu†

Department of Physics, Southeast University, Nanjing 210096, China and

Department of Physics, South University of Science and Technology of China, Shenzhen 518055, China

Recently, the topological valley current flowing in the gapped graphene was observed in a four-terminal Hall-bar device by measuring the nonlocal resistivity signal [Gorbachev *et al.*, Science **346**, 448 (2014)]. In this work, we study numerically the quantum valley Hall effect in the same Hall bar geometry based on a lattice model and the multiple-terminal Landauer-Büttiker formula. It is found that in the clean limit, the nonlocal resistivity R_{NL} is quantized, $R_{NL} = h/e^2$, as long as the Hall-bar width exceeds its length $w > l$ and in the opposite case $l > w$, it decreases exponentially, $R_{NL} \sim e^{-l/w}$. The quantization of R_{NL} originates from the quantized valley Hall conductivity of the gapped graphene, while its requirement of $w > l$ relates to the fact that the valley degree of freedom is defined in the reciprocal space and sensitive to the device profile. The quantization of R_{NL} is also shown robust against both the rough edges of graphene and static disorders. Our findings may shed light on the fabrication of valley-based devices.

PACS numbers: 72.80.Vp, 72.10.Bg, 73.43.-f, 85.75.-d

I. INTRODUCTION

Similar to spintronics, valleytronics is a new rising discipline and referred to as the electronics based on the valley degree of freedom (*d.o.f.*) of electrons in 2D honeycomb lattice systems[1–3]. It is believed that the valleytronics device, similar to the spintronics device, shall have a lower energy consumption, faster processing speed, and higher integration density in comparison to the traditional charge-based electronic device. The valley refers to each of the energetically degenerate, but nonequivalent structures in the energy bands of crystalline materials. A typical example is the monolayer graphene that has two valleys in the reciprocal space, denoted as the $\mathbf{K}$ and $\mathbf{K}'$ valley, respectively, and they are related by the time reversal symmetry like the spin *d.o.f.* of electrons. Due to the large momentum difference between the two valleys in graphene, the intervalley scattering is severely suppressed[4–7] in clean samples and the valley is largely a conserved quantum number in electron transports. Thus, it is suggested that the valley could be utilized as an information carrier.

Since the valleytronics is still in its infancy, the main challenges in this field are the generation, detection, and manipulation of valley currents. Many proposals have been studied to generate valley currents by using

graphene nanoribbon[8–10], lattice strain[11–17], electromagnetic field[16–24], optical field[25–27], and line defects[28–30]. A pseudovalley-exchange interaction was also proposed by authors[31] in the graphene superlattice system to modulate the valley state. As for the valley detection, the usual way is the optical excitation method based on the valley-dependent selection rule[32,33]. Very recently, three groups have successfully and independently measured the topological valley current flowing in the monolayer[34] or bilayer graphene[35,36] by a purely electric means via the inverse quantum valley Hall effect (QVHE).

As is known, the monolayer graphene with broken inversion symmetry is a quantum valley Hall insulator[3], i.e., a quantized valley Hall current can be induced by a longitudinal electric field $\mathbf{E}$, because electrons undergo a momentum deflection due to the nonzero Berry curvature of massive Dirac electrons that resembles a magnetic field rotating a moving charge. The Berry curvatures in the $\mathbf{K}$ and $\mathbf{K}'$ valleys are opposite to each other, so that the valley Hall current is a pure valley current without any accompanied charge current. As a result, the experimental observation of such valley Hall current is generally to utilize the inverse QVHE to transform it nonlocally into a measurable voltage or current signal, similar to the measurement of the pure spin current. Gorbachev *et al.*[34] measured a strong nonlocal resistivity signal at the charge neutral point of the graphene in a four terminal Hall-bar device, where the monolayer graphene was placed on the hexagonal Boron Nitride and an energy gap at Dirac points is opened. While the measured nonlocal resistivity R_{NL} represents the topological valley current generated via the QVHE, an important issue remains intact why the measured R_{NL} is not quantized when the Fermi energy resides in the energy gap, since the valley Hall conductivity is quantized. Generally speaking, the conductance or resistivity quantization in a quantum Hall effect shall be very robust and not difficult to detect. Thus, it is desirable to find the discrepancy between the experimental observation[34] and theoretical prediction[3] of the QVHE.

In this work, we study numerically the experimental four-terminal Hall-bar device of a gapped monolayer graphene, which is denoted by a staggered potential applied to the carbon A and B sites. The nonlocal resistivity is calculated according to the multiterminal Landauer-Büttiker formula in the linear transport regime. In the clean limit, we show that the quantized $R_{NL} = h/e^2$ is possible when the Hall-bar width is larger than its length ($l < w$) and the Fermi energy resides in the energy gap. In the opposite case $w < l$, the quantized R_{NL} are severely destroyed and exponentially decreases to zero, $R_{NL}{\sim}e^{-l/w}$. This is consistent with the experiment result[34] that the quantized R_{NL} can be extrapolated from the measured data at the limit of $l \sim 0$. Outside of the bulk energy gap, the R_{NL} is shown to be very sample-parameter dependent, but cannot exceed the quantized one ($R_{NL} < h/e^2$). The quantized R_{NL} is also shown immune to the rough edges of the

device and static disorders.

This work is organized as follows. In Sec. II, the Hall-bar device based on a lattice model is outlined and the numerical method to the nonlocal resistivity is presented. Numerical results are given in Sec. III and the origin of the quantized R_{NL} is also discussed in detail. A brief conclusion is drawn in the last section.

II. MODEL

Before we describe our model to calculate the nonlocal resistivity induced by the combined QVHE and inverse QVHE, we first recall the QVHE physics in a gapped graphene. In order to open an energy gap of the massless Dirac electrons with a linear energy dispersion, a staggered potential breaking the inversion symmetry of graphene is often introduced in the lattice. Experimentally, the general method is to deposit the graphene on the hexagonal Boron Nitride layer due to the very lattice match. The low-energy continuum Hamiltonian of graphene without the inversion symmetry[3] is given by

$$H = v_F(\sigma_x \hat{p}_x + \sigma_y \hat{p}_y \tau_z) + \Delta\sigma_z, \qquad (2.1)$$

where $\sigma_{i=x,y,z}$ are the Pauli matrices of the lattice pseudospin, $\hat{p}_{x,y}$ are the momentum operators; $\tau_z = \pm 1$ denotes the $\mathbf{K}$ and $\mathbf{K}'$ valleys; v_F is the Fermi velocity; the last term is the staggered potential with its strength Δ denoting the site-energy difference between carbon A and B atoms. Here the real spin is neglected and assumed degenerate in this work. From the eigenvalue $E = \pm\sqrt{v_F^2(p_x^2 + p_y^2) + \Delta^2}$ of the above Hamiltonian, an energy gap with its width 2Δ is seen at the Dirac point and the gapped graphene is insulating.

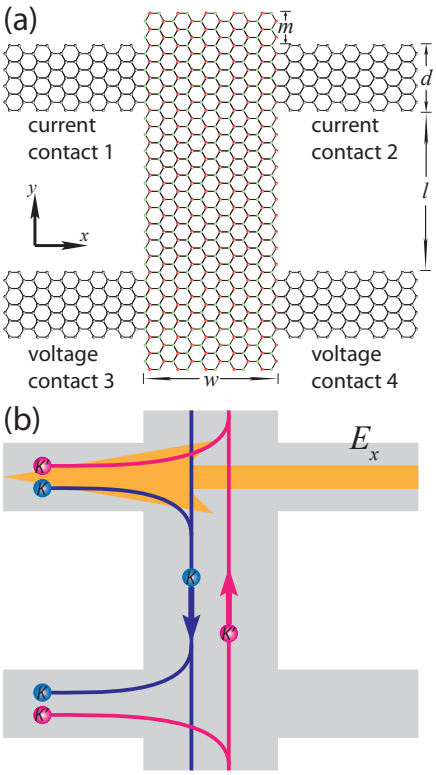

FIG. 1: (Color online) (a) Schematic of a Hall-bar graphene setup with the armchair termination. The upper two leads (lead 1 and 2) are the current contacts and the lead 3 and 4 are the two voltage probes. w is the Hall-bar width and l is its length representing the distance between the current and voltage contacts, and m denotes the extended length of the H shape device. (b) Plot of the QVHE and inverse QVHE processes for the generation of a nonlocal voltage signal. A valley current is flowing along the y-axis direction due to the QVHE induced by the electric field E_x, and a voltage signal is generated between the lead 3 and 4 due to the inverse QVHE.

Using the Kubo formula for the d.c. Hall conductivity,

$$\sigma_{xy} = \frac{ie^2\hbar}{S} \sum_{\xi\xi'(\xi\neq\xi')} \frac{[f(\varepsilon_\xi) - f(\varepsilon_{\xi'})]\langle\xi|v_x|\xi'\rangle\langle\xi'|v_y|\xi\rangle}{(\varepsilon_\xi - \varepsilon_{\xi'})^2}, \tag{2.2}$$

where S is the volume and $\hat{v}_{x(y)} = \frac{\partial H}{\partial \hat{p}_{x(y)}}$, ε_ξ and $|\xi\rangle$ are the eigenvalue and eigenfunction of the system with ξ being the quantum number, respectively; $f(\varepsilon_\xi)$ is the Fermi-Dirac distribution function. One can directly derive out the valley-related Hall conductivity[3] as $\sigma_{xy}^{\tau_z} = \tau_z(1 - \Delta/2E)e^2/h$ with E being the Fermi energy, and the valley Hall conductivity is quantized as $\sigma_{xy}^v = \sigma_{xy}^K - \sigma_{xy}^{K'} = e^2/h$, when the Fermi energy is in the energy gap $|E| < \Delta$.

The Kubo formula above can be also written as $\sigma_{xy} = \frac{e^2}{h}\int \frac{d\mathbf{k}}{2\pi} f(\varepsilon_\mathbf{k})\Omega(\mathbf{k})$, where $\Omega(\mathbf{k})$ is the Berry curvature of massive Dirac electrons accounting for the momentum deflection with the help of an external electric field. All physics variables in the Hall conductivity formula above [Eq. (2)] is independent of the electric field $\mathbf{E}$, since the system is assumed to be in an equilibrium state (without interactions from the external electric field $\mathbf{E}$) required by the linear response theory. In other words, the valley Hall conductivity σ_{xy}^v should not depend explicitly on the electric field and can be evaluated without $\mathbf{E}$ considered in the equilibrium Hamiltonian. Certainly, the valley Hall current J_y^v will rely on the longitudinal electric field E_x, $J_y^v = \sigma_{xy}^v E_x$. Therefore, the Landauer-Büttiker formula in the linear transport regime can be used to calculate this valley Hall conductivity σ_{xy}^v in principle. As a matter of fact, the Landauer-Büttiker formula for a simple two-terminal device can be derived from the linear response theory and the behind physics is that the transport properties of the system are generally determined by the electrons near Fermi energy.

The gapped graphene is actually a valley Chern insulator[3], $\sigma_{xy}^v = \frac{e^2}{h}C_v$, where $C_v = 1$ is the valley Chern number, so a longitudinal electric field $\mathbf{E}$ can lead to a topologically-protected valley Hall current. It is noted that unlike the charge or spin Chern insulator, there is no edge state along the boundary of the sample supporting dissipationless valley currents, because the vacuum (insulator) has no such valley definition[37]. An indirect method is needed to measure the valley current, and thus the four-terminal Hall-bar device is usually employed to detect the QVHE by measuring the nonlocal resistivity R_{NL}. In the schematic setup plotted in Fig. 1(a), the contact 1 and 2 are assumed to be the current contacts, upon which an external bias $V_1 - V_2$ is applied. While the contact 3 and 4 are the voltage probes through which no electric current is flowing. A pure valley current shall first be generated to flow along the y-direction via the QVHE, and then it will be transformed into a voltage signal in contact 3 and 4 due to the inverse QVHE, this is schematically drawn in Fig. 1(b). Due to the lack of edge stats, the longitudinal conductivity of the gapped graphene is zero ($\sigma_{xx} = 0$) although the valley Hall conductivity is quantized $\sigma_{xy}^v = e^2/h$, so the nonlocal resistivity should also be quantized in terms of the reversibility, $R_{NL} = (\sigma_{xy}^v)^{-1} = h/e^2$. However, the current exper-

iment (Ref.[34]) failed to observe directly this quantized R_{NL}.

A tight-binding Hamiltonian is employed to describe the gapped graphene in Fig. 1(a)

$$\mathcal{H} = \sum_{\langle ij \rangle} (t C_i^\dagger C_j + h.c.) + \sum_i \mu_i \Delta C_i^\dagger C_i, \qquad (2.3)$$

where the first term represents a pristine graphene, $\langle ij \rangle$ is the summation over the nearest-neighbor A and B carbon atoms, t is the electron's hopping strength, $C_i^\dagger$ (C_j) is the creation (annihilation) operator at the lattice site i (j); the second term is the staggered potential accounting for the possible energy gap opened at the Dirac points, $u_i = \pm 1$ ($i = A, B$). The staggered potential Δ is only applied to the scattering region of the device and absent in the four ideal graphene leads. The multi-terminal Landauer-Büttiker formula in the linear transport regime is used to calculate the nonlocal resistivity R_{NL}. The current in each lead p is given by

$$I_p = \frac{e^2}{h} \sum_q T_{pq}(V_p - V_q), \qquad (2.4)$$

where $V_{p(q)}$ are the voltage in contact $p, q = 1, 2, 3, 4$, and T_{pq} is the electron transmission at the Fermi energy between the lead p and q, $T_{pq} = Tr[\Gamma_p G^r \Gamma_q G^a]$ with $G^{r(a)}$ being the retarded (advanced) Green's function of the system. $G^r(E) = [G^a(E)]^\dagger = [EI - \mathcal{H} - \sum_p \Sigma_p^r]^{-1}$, where I is the unit matrix, Σ_p^r is the self-energy of each contact p, $\Gamma_p = i(\Sigma_p^r - (\Sigma_p^r)^\dagger)$, $\mathcal{H}$ is the Hamiltonian of the gapped graphene in the scattering region, and the trace is over the matrix dimension of the Hamiltonian. In the device of Fig. 1(a), we have $I_1 = -I_2$ due to the current conservation, and $I_3 = I_4 = 0$ because they are the voltage probes. It is not difficult to work out the voltage V_3 and V_4 in terms of the bias $V_1 - V_2$. Then, the nonlocal resistivity is defined as

$$R_{NL} = \frac{V_3 - V_4}{I_1}. \qquad (2.5)$$

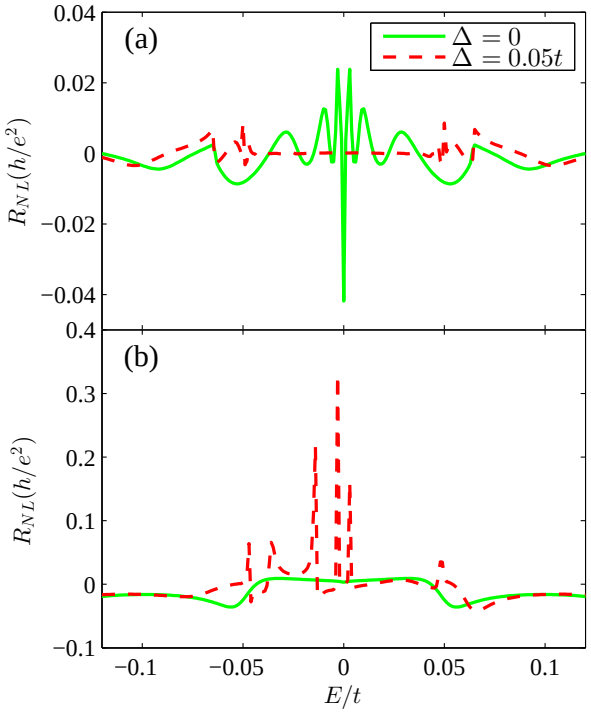

FIG. 2: (Color online) Nonlocal resistivity R_{NL} versus the Fermi energy E in a nanosize Hall-bar graphene geometry with either the armchair-edge (a) or zigzag-edge (b) termination. Parameters are $d = l = w = 5$ nm and $m = 0$.

III. RESULTS AND DISCUSSIONS

In this section, we will carry out the numerical calculations of R_{NL} as functions of the device parameters according to the above formulae. The four ideal graphene leads are assumed identical with the same width d, the

Hall-bar length l denotes the distance between the current contacts (lead 1, 2) and voltage probes (lead 3, 4), and w is the width of the Hall bar as depicted in Fig. 1(a). In numerics, the hopping energy of electrons in graphene[38] is set as $t = 2.8$ eV, zero temperature is assumed in our calculations, and the lattice constant is set as $a = 2.46\mathring{A}$. The graphene edges of the device can be arbitrary, both the zigzag and armchair types are taken for convenience in computations.

We first present numerical results of R_{NL} in the nanosize Hall-bar device as a function of the Fermi energy E. It is shown in Fig. 2 that a nonzero R_{NL} indeed appears irrespective of zero or nonzero staggered potential Δ in the graphene and exhibits extreme sensitivity to the system parameters. This agrees with a recent work[39] that a nonzero R_{NL} was found in the nanosize graphene without an energy gap. For the armchair-edge device [Fig. 2(a)], the R_{NL} takes its maximum at the neutral point when $\Delta = 0$, whereas R_{NL} disappears nearly in the zigzag-edge case [Fig. 2(b)]. Moreover, R_{NL} can be positive or negative for different Fermi energies and different edge types of graphene. All these indicate that in the nanosize device, the electron scattering at the boundaries of the sample should dominate the nonlocal resistivity and the obtained R_{NL} should not exclusively denote the topological valley current generated by QVHE. Especially, the nonzero R_{NL} at the pristine graphene ($\Delta = 0$ and there is no QVHE) can merely stem from the intervalley scattering at the boundaries of the sample or the possible pseudolattice spin Hall effect.

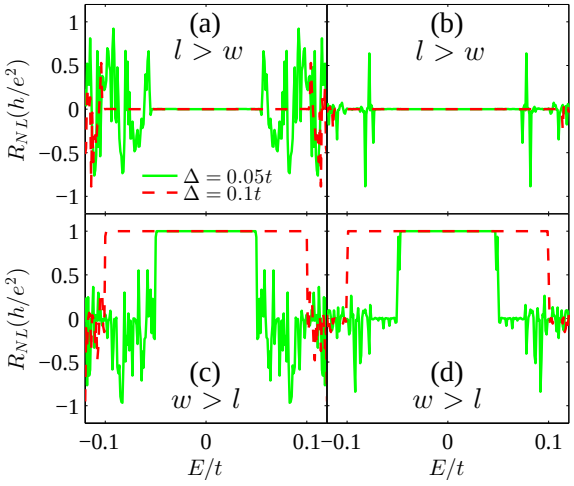

FIG. 3: (Color online) Nonlocal resistivity R_{NL} as a function of the Fermi energy E in the armchair-edge (a) and (c), and zigzag-edge (b) and (d) device. $l = 200$ nm and $w = 50$ nm for the upper two panels (a) and (b), and $w = 200$ nm and $l = 50$ nm for the lower two panels (c) and (d). Other parameters are $d = 50$ nm and $m = 0$ nm.

We proceed to consider a much larger device of hundreds of nanometers, and present the numerical results in Fig. 3, since the larger the graphene size is, the better the $\mathbf{K}$ and $\mathbf{K}'$ valleys are defined. The left two panels [Fig. 3(a) and 3(c)] are plotted for the zigzag-edge device and the right two [Fig. 3(b) and 3(d)] for the armchair-edge graphene. In the upper two panels, the case of $l > w$ is shown and a nonlocal signal of R_{NL} appears, $R_{NL} \neq 0$. However, R_{NL} nearly vanishes in the energy gap $\Delta > |E|$ and irregularly oscillates when $|E| > \Delta$. When the l and w are reversed, $l < w$ in Fig. 3(c) and 3(d), the R_{NL} shows a quantization platform ($R_{NL} = h/e^2$) when the Fermi energy resides in

the energy gap $|E| < \Delta$. The platform width is exactly equal to the energy gap width 2Δ. R_{NL} exhibits similar irregular oscillations when $|E| > \Delta$.

For both types of graphene edges in Fig. 3, the quantization is the same. In fact, other chiral edges of graphene (mixture of the zigzag and armchair types) as well as different graphene or nongraphene leads do not change this quantization a little (not shown). Additionally, the extension length m of the device in Fig. 1(a) does not affect the quantization of R_{NL}, either, and thus neglected in our calculations. Since the quantization of R_{NL} is not sensitive to small variation of the sample parameters, it should not come from very parameter-dependent scattering of electrons but the intrinsic QVHE. One can see $R_{NL}(E) = R_{NL}(-E)$ from Fig. 3, and this is consistent with the valley Hall conductivity $\sigma^v_{xy}(E) = \sigma^v_{xy}(-E)$ different from the usual Hall conductivity.

Since the quantization of R_{NL} is closely dependent on the relative magnitudes of w and l of the studied Hall-bar structure, we compute R_{NL} with variation of l and w and present the results in Fig. 4(a). It is seen that for a fixed w, $R_{NL} = h/e^2$ remains unchanged roughly at $l < w$, whereas it is destroyed at the case of $l > w$ and will exponentially decrease. This phase-transition behavior, $e^2R_{NL}/h = 1$ or $R_{NL} \simeq 0$, occurs in the whole energy gap $|E| < \Delta$. Alternatively, the critical length l_c for quantized R_{NL} is independent of energy E as long as it resides in the gap $|E| < \Delta$.

We can work out the critical length l_c defined as the exponential decay length of R_{NL} and a phase diagram is plotted in Fig. 4(b). It is seen that the l_c approximates to w in a comparatively large device, $l_c \simeq w$, except for the onset point $l \sim 0$. This relationship is nearly independent of the lead width d used in calculations [Fig. 4(b)] as well as the edge types of the device. Therefore, we have the relationship $R_{NL} \sim e^{-l/w}$. Certainly, the transport here is entirely controlled by quantum theory in the clean limit and not in the diffusive regime. The experimental observation of the valley diffusive length[34] $\xi_v \simeq w$, which is valid even for bilayer graphene[35,36], might relate to this quantum confinement requirement, $l_c \simeq w$. As a matter of fact, the quantized $R_{NL} = h/e^2$ at $l \sim 0$ can be extrapolated from the experimentally measured data[34], and this is consistent with our results.

We have shown that the Hall-bar width w is a crucial factor for the quantized R_{NL} and even at the limit of $l \ll w$, $R_{NL} = h/e^2$ is still valid. Before elaborating its origin, we should keep in mind that the topological valley current (quantized valley conductivity, $\sigma^v_{xy} = e^2/h$) generated via the QVHE is not related to any edge states, but sustained by the whole valence band[40], because there is no topologically-protected edge state in the gapped graphene, even for a finite-size device we studied here. In the following, we present an intuitive interpretation of the condition $l_c \sim w$ for quantized $R_{NL} = h/e^2$.

It is assumed that a valley current arising from the QVHE is flowing along the y-direction in Fig. 1(b). For the electron moving in the narrow Hall-bar region,

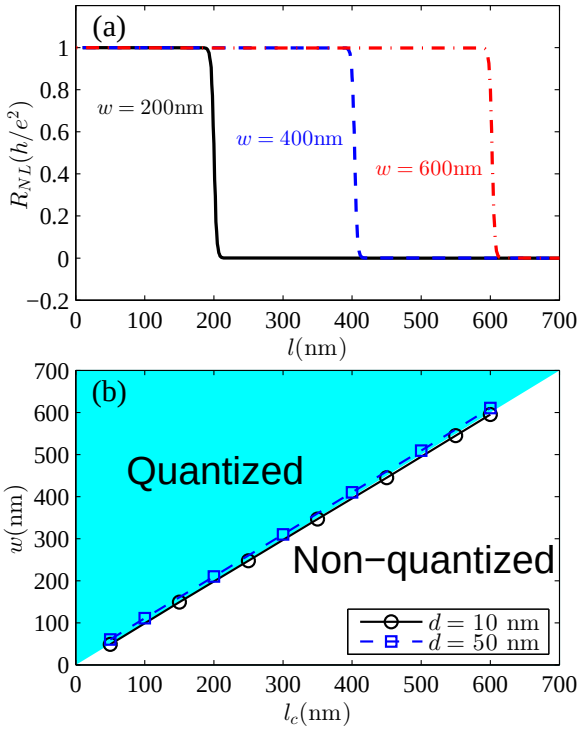

FIG. 4: (Color online) (a) Nonlocal resistivity R_{NL} in the energy gap as a function the Hall-bar length l with different w. (b) Critical length l_c for the quantized R_{NL} versus the Hall-bar width w. The zigzag-edge device edge is considered here and the armchair-edge one has the same result (not shown). Parameters are $d = 50$ nm, $\Delta = 0.1t$, $m = 0$ nm, and $E = \Delta/2$.

$w > \lambda_x$ is required for a complete transverse mode, where λ_x is the x-component wavelength of the electron, while there is no such limitation for the longitudinal wavelength λ_y, because the electrodes are posited at the two ends of the length l. Those electrons' momenta will be deflected by the Berry curvature in the inverse QVHE process, and meanwhile, the electron energy E is assumed to be conserved in the transport, so the λ_y and λ_x approximately exchange to each other in this inverse QVHE process. Not all electrons can directly complete such energy-conserved momentum deflection or interchange when $l > w$, and those $\lambda_y > w$ wave quantum states shall necessarily involve the superposition of different waves including different valleys. It is this intervalley scattering that leads to the exponential decrease of R_{NL} in Fig. 4(b), as a result, the transport of the inverse QVHE is actually in the diffusive regime, although no defect or disorder was considered in our calculations. For the opposite case $l < w$, all waves including the maximum waves $\lambda_x \sim w$ can be deflected into the λ_y wave transporting along the y direction, i.e., all electrons can successfully complete the QVHE process at $w > l$, so the R_{NL} is quantized at $|E| < \Delta$. We wish to point out that the electron deflection may bring about the intervalley scattering, because the the valley *d.o.f* unlike the spin or charge, is defined in the reciprocal space and thus closely related to the graphene lattice profile, e.g., the electron wavevector $(k_x\hat{x},\ k_y\hat{y})$ is given by $(n_x\frac{2\pi}{w},\ n_y\frac{2\pi}{l})$ in the Brillouin zone with $n_{x(y)}$ being an integer, and then, the momentum exchange or rotation $(k_y\hat{x},\ k_x\hat{y})$ cannot ensure the deflected electron staying in the same valley, when the width and length $(w,\ l)$ of a graphene device are not matched very well.

The above results are based on the pure quantum transport in the clean limit. In the following, we proceed to study the disorder effect on the nonlocal resistivity R_{NL}. Generally, the long-ranged interaction like charge impurities shall not provide intervalley scattering due to

the large momentum difference between the **K** and **K′** valleys, whereas the short-ranged one can indeed contribute to the intervalley scattering. Here, we consider the harder case, short-ranged disorders in the graphene lattice. In calculations, each carbon site on the sample assumes a random on-site energy in the range of $[-D,D]$, where D is the disorder strength, the four contacts still keep clean without any disorder, and the results are averaged over 800 disorder configurations.

In Fig. 5, the R_{NL} is plotted with a variation of the disorder strength D. One can see that the R_{NL} can easily be suppressed when $|E| > \Delta$, but the quantized platform displays quite robust against disorder. Around the band center $E = 0$, the R_{NL} quantization is much stronger than that at the band edge $|E| \sim \Delta$. As discussed earlier, the nonzero R_{NL} signal outside of the energy gap ($|E| > \Delta$) has the contribution from the electron's scattering that is sensitive to the sample parameters such as the Fermi energy, size, and edge types, subsequently, the disorder can easily get rid of such oscillation of R_{NL}. It is also shown in Fig. 5(b) that the R_{NL} at $|E| > \Delta$ will decrease to zero around $D \sim \Delta$ and then will continuously increase at $D > \Delta$ because of the closure of the bulk energy gap of graphene.

For $|E| < \Delta$, the R_{NL} is only generated via the QVHE so that it should be protected by the topology of the gapped graphene and immune to a moderate disorder. The behavior of R_{NL} versus Δ in Fig. 5(b) confirms this point. The R_{NL} at the charge neutral point can survive in a much stronger disorder environment, $D \sim 10\Delta$. This is not found in other topological insulators, e.g. the quantized conductance of the helical edge states in a quantum spin Hall insulator can only survive in the disorder with the strength lesser than the bulk energy gap. There are two concerning factors that may account for the extremely strong R_{NL}: one is that the R_{NL} is contributed by the whole valence band[40] and the gapped graphene (quantum valley Hall insulator) has no gapless edge state; the other comes from the fact that the valley conductivity is an even function of the energy E different from other Hall effects, $\sigma^v_{xy}(E) = \sigma^v_{xy}(-E)$, the charge fluctuation due to disorder cannot smash the R_{NL} greatly.

The obtained results of R_{NL} dependence on the disorder is quite different from a recent work by Ando[41], who found that the valley Hall conductivity σ^v_{xy} by using a low-energy continuum model can be enhanced by disorder when $|E| > \Delta$, and even be larger than the quantized one $\sigma^v_{xy} = e^2/h$. This immediately implies that the R_{NL} should also increase with the disorder. However, the R_{NL} at $|E| > \Delta$ here is suppressed greatly instead of enhancement as shown in Fig. 5(b) when the disorder is no too strong $D \sim \Delta$. The R_{NL} increases with disorder only when $D > \Delta$ but cannot exceed the quantized value. In this strong disorder case, the energy gap of the graphene shall be closed by the disorder and the nonlocal R_{NL} signal mainly come from the electron scattering or the pseudolattice spin Hall effect. This situation is

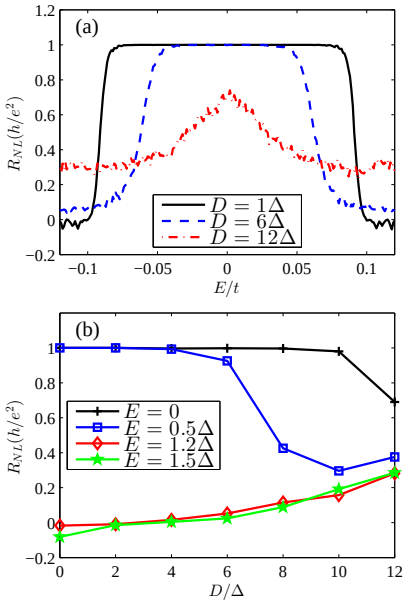

FIG. 5: (Color online) (a) Plot of the nonlocal resistivity R_{NL} as a function of the Fermi energy E within different disorder strengths. (b) R_{NL} versus the disorder strength D for different Fermi energies. Parameters are $d = 30$ nm, w= 100 nm, $l = 50$ nm, and $\Delta = 0.1t$.

the same as the nonzero R_{NL} at $\Delta = 0$ found in Fig. 2. Therefore, the increasing of R_{NL} with D for $|E| > \Delta$ in Fig. 5(b) shall arise from the effect of the electron scattering at the device boundary, not fully from the QVHE found in Ref.[41]. Certainly, the sample boundary is the main difference considered in our model from Ref.[41], and therefore, it should be an important factor to be seriously taken into account in making valley-based devices.

IV. CONCLUSION

In summary, we have numerically investigated the QVHE in the gapped graphene by calculating the nonlocal resistivity in a Hall-bar structure. Based on a lattice model and the multiple-terminal Landauer-Büttiker formula, we have shown that the nonlocal resistivity is quantized $R_{NL} = h/e^2$ representing the QVHE when the Hall-bar length is smaller than its width ($l < w$) and the Fermi energy resides in the bulk energy gap $|E| < \Delta$, and it decreases rapidly at the $l > w$ case, $R_{NL} \sim e^{-l/w}$. This is attributed to the fact that the valley $d.o.f$ is defined in the reciprocal space and the electron deflection in real space by the nonzero Berry curvature may lead to the intervalley scattering. The quantized R_{NL} is not sensitive to other system parameters such as graphene-edge types and is also shown very robust against static disorders. Our results are useful for future fabrication of valley-based devices.

Acknowledgments

The work described in this paper is supported by NSFC (Grant No. 11274059 and 11204187) and the NSF of Jiangsu Province (Grant No. BK20131284).

* Electronic address: jwang@seu.edu.cn

† Electronic address: liujf@sustc.edu.cn

[1] D. Pesin and A. H. MacDonald, Nat. Mater. **11**, 409 (2012).

[2] K. Behnia, Nat. Nanotech. **7**, 488 (2012).

[3] D. Xiao, W. Yao, and Q. Niu, Phys. Rev. Lett. **99**, 236809 (2007).

[4] A. F. Morpurgo and F. Guinea, Phys. Rev. Lett. **97**,

196804 (2006).

[5] S. V. Morozov, K. S. Novoselov, M. I. Katsnelson, F. Schedin, L. A. Ponomarenko, D. Jiang, and A. K. Geim, Phys. Rev. Lett. **97**, 016801 (2006).

[6] R. V. Gorbachev, F. V. Tikhonenko, A. S. Mayorov, D. W. Horsell, and A. K. Savchenko, Phys. Rev. Lett. **98**, 176805 (2007).

[7] J.-H. Chen, W. G. Cullen, C. Jang, M. S. Fuhrer, and E. D. Williams, Phys. Rev. Lett. **102**, 236805 (2009).

[8] A. Rycerz, J. Tworzydlo, and C. W. J. Beenakker, Nat. Phys. **3**, 172 (2007).

[9] A. R. Akhmerov, J. H. Bardarson, A. Rycerz, and C. W. J. Beenakker, Phys. Rev. B. **77**, 205416 (2008).

[10] H. Schomerus, Phys. Rev. B **82**, 165409 (2010).

[11] F. Zhai and K. Chang, Phys. Rev. B **85**, 155415 (2012).

[12] Z.-Z. Cao, Y.-F. Cheng, and G.-Q. Li, Appl. Phys. Lett. **101**, 253507 (2012).

[13] T. Fujita, M. B. A. Jalil, and S. G. Tan, Appl. Phys. Lett. **97**, 043508 (2010).

[14] T. Low and F. Guinea, Nano Lett. **10**, 3551 (2010).

[15] Z. Khatibi, H. Rostami, and R. Asgari, Phys. Rev. B **88**, 195426 (2013).

[16] Z. Wu, F. Zhai, F. M. Peeters, H. Q. Xu, and K. Chang, Phys. Rev. Lett. **106**, 176802 (2011).

[17] Y. Jiang, T. Low, K. Chang, M. I. Katsnelson, and F. Guinea, Phys. Rev. Lett. **110**, 046601 (2013).

[18] L. E. Golub, S. A. Tarasenko, M. V. Entin, and L. I. Magarill, Phys. Rev. B **84**, 195408 (2011).

[19] G. Y. Wu, N.-Y. Lue, and Y.-C. Chen, Phys. Rev. B **88**, 125422 (2013).

[20] J. Wang, K. S. Chan, and Zijing Lin, Appl. Phys. Lett. **104**, 013105 (2014).

[21] S. K. Wang, J. Wang, and K. S. Chan, New J. Phys. **16**, 045015 (2014).

[22] A. Chaves, L. Covaci, Kh. Yu. Rakhimov, G. A. Farias, and F. M. Peeters, Phys. Rev. B **82**, 205430 (2010).

[23] J. Wang and S. Fischer, Phys. Rev. B **89**, 245421 (2014).

[24] M. M. Grujić, M. Ž. Tadić, and F. M. Peeters, Phys. Rev. Lett. **113**, 046601 (2014).

[25] A. Kundu, H. A. Fertig, and B. Seradjeh Phys. Rev. Lett. **116**, 016802 (2016).

[26] H. L. Zeng, J. F. Dai, W. Yao, D. Xiao, and X. D. Cui, Nat. Nanotech. **7**, 490 (2012).

[27] W. Yao, D. Xiao, and Q. Niu, Phys. Rev. B. **77**, 235406 (2008)

[28] D. Gunlycke and C. T. White, Phys. Rev. Lett. **106**, 136806 (2011).

[29] Y. Liu, J.-T. Song, Y.-X. Li, Y. Liu, and Q.-F. Sun, Phys. Rev. B **87**, 195445 (2013).

[30] J.-H. Chen, G. Autès, N. Alem, F. Gargiulo, A. Gautam, M. Linck, C. Kisielowski, O. V. Yazyev, S. G. Louie, and A. Zettl, Phys. Rev. B **89**, 121407(R) (2014).

[31] S. K. Wang and J. Wang, Phys. Rev. B **92**, 075419 (2015).

[32] T. Cao, G. Wang, W. Han, H. Ye, Ch. Zhu, J. Shi, Q. Niu, P. Tan, E. Wang, B. Liu, and J. Feng, Nat. Commun. **3**, 887 (2012).

[33] K. F. Mak, K. He, J. Shan, and T. F. Heinz, Nat. Nanotechnol. **7**, 494 (2012).

[34] R. V. Gorbachev, J. C. W. Song, G. L. Yu, A. V. Kretinin, F. Withers, Y. Cao, A. Mishchenko, I. V. Grigorieva, K. S. Novoselov, L. S. Levitov, and A. K. Geim, Science **346**, 448 (2014).

[35] M. Sui, G. Chen, L. W. Shan, D. Tian, K. Watanabe, T. Taniguchi, X. Jin, W. Yao, D. Xiao, and Y. Zhang, Nat.

Phys. **11**, 1027 (2015).

[36] Y. Shimazaki, M. Yamamoto, I. V. Borzenets, K. Watanabe, T. Taniguchi, and S. Tarucha, Nat. Phys. **11**, 1032 (2015).

[37] M. Ezawa, Phys. Rev. B **88**, 161406(R) (2013).

[38] L. Pisani, J. A. Chan, B. Montanari, and N. M. Harrison, Phys. Rev. B **75**, 064418 (2007).

[39] G. Kirczenow, Phys. Rev. B **92**, 125425 (2015).

[40] Y. D. Lensky, J. C.W. Song, P. Samutpraphoot, and L. S. Levitov, Phys. Rev. Lett. **114**, 256601 (2015).

[41] T. Ando, J. Phys. Soc. Jap. **84**, 114705 (2015).